論文 / 著書情報
Article / Book Information

Title	Ex-situ Analysis of Lithium Distribution in a Sulfide-based All-solid-state Lithium Battery by Particle-induced X-ray and Gamma-ray Emission Measurements
Authors	Yuto Yamada, Kota Suzuki, Kazuhiro Yoshino, Sou Taminato, Takahiro Satoh, Martin Finsterbusch, Tomihiro Kamiya, Akiyoshi Yamazaki, Yoshiaki Kato, Kazuhisa Fujita, Kunioki Mima, Satoshi Hori, Masaaki Hirayama, Ryoji Kanno
Citation	Electrochemistry, volume 88, Issue 1, Pages 45-49
Pub. date	2020, 1
Note	This file is author (final) version.

Ex-situ analysis of lithium distribution in a sulfide-based all-solid-state lithium battery by particle-induced X-ray and gamma-ray emission measurements

Yuto. YAMADA[a], Kota. SUZUKI[a,b]*, Kazuhiro. YOSHINO[a], Sou. TAMINATO[c], Takahiro. SATOH[d], Martin. FINSTERBUSCH[e], Tomihiro. KAMIYA[f], Akiyoshi. YAMAZAKI[g], Yoshiaki. KATO[h], Kazuhisa. FUJITA[h], Kunioki. MIMA[h], Satoshi. HORI[b], Masaaki. HIRAYAMA[a,b] and Ryoji. KANNO[a,b]

[a]Department of Chemical Science and Engineering, School of Materials and Chemical Technology, Tokyo Institute of Technology, 4259 Nagatsuta, Midori-ku, Yokohama 226-8502, Japan

[b]Institute of Innovative Research (IIR), Tokyo Institute of Technology, 4259 Nagatsuta, Midori-ku, Yokohama 226-8502, Japan

[c]Department of chemistry for Materials, Mie University, 1577 Kuriyamachiya-cho, Tsu, Mie 514-8507 Japan

[d]National Institutes for Quantum and Radiological Science and Technology, 1233 Watanuki-machi, Takasaki, Gunma 370-1292, Japan

[e]Forschungszentrum Jülich GmbH, represented by its Board of Directors, for: Institute of Energy and Climate Research (IEK-1), Wilhelm-Johnen-Straße, 52428 Jülich, Germany

[f]Graduate School of Science and Technology. Gunma University, 1-5-1 Tenjin-cho, Kiryu, Gunma 376-8515, Japan

[g]Faculty of Pure and Applied Sciences, University of Tsukuba, 1-1-1 Tennodai, Tsukuba, Ibaraki 305-8577, Japan

K. Tokyo

[h]The Graduate School for the Creation of New Photonics Industries, 1955-1, Kurematsu, Nishi-ku, Hamamatsu, Shizuoka 431-1202, Japan

* Corresponding author : ksuzuki@echem.titech.ac.jp

ABSTRACT

Lithium distribution in the composite electrode of an all-solid-state lithium battery was analyzed by microbeam-particle-induced X-ray emission and gamma-ray emission techniques. Two kinds of pellet-type cells, incorporating $LiCoO_2$ as the cathode-active material and the superionic conductor $Li_{10}GeP_2S_{12}$ as the solid electrolyte, were prepared: one in the as-prepared state and the other in the charged state. Changes in lithium distribution near the interface between the composite cathode and separator were visualized by normalization of lithium/cobalt intensity. Lithium extraction from $LiCoO_2$ due to charging was confirmed by the decrease in normalized intensity at the cathode composite region. The evaluation of the lithium concentration variation in the composite electrode for the all-solid-state battery during the electrochemical reactions could provide essential information for construction of a favorable composite electrode to enable preparing high-performance all-solid-state lithium batteries.

Keywords: PIGE, PIXE, Lithium distribution, All-solid-state lithium battery

1. Introduction

All-solid-state lithium batteries using inorganic solid electrolytes have vast potential as energy storage candidates beyond the conventional lithium battery because of benefits, such as high power density, thermal stability, and the lack of electrolyte leakage. These features are predicted to be vital for the development of the highly sought after next-generation high-power energy devices.[1] The availability of solid electrolytes with extremely high ionic conductivity is a critical requirement for the construction of high-performance all-solid-state batteries. In recent years, sulfide-based solid lithium-ion conductors exhibiting remarkably high ionic conductivity have attracted attention as solid electrolyte candidates for the development of high-performance all-solid-state batteries. Particularly, $Li_{10}GeP_2S_{12}$-type materials[2, 3], Li_2S-P_2S_5 glass ceramic[4], and argyrodite-type materials are highly preferred solid electrolytes because of their high ionic conductivities ($>10^{-2}$ S cm^{-1} at 300 K). Additionally, sulfide-based materials possess favorable mechanical properties for realizing efficient contact with active materials due to their good plastic deformability[5]. However, unlike the liquid electrolyte, the solid electrolyte does not automatically penetrate the voids of electrode powders. To address this, several fabrication studies have been conducted for improving this aspect of the composite electrode [6-9]. Since the obtained composite structures, and the performance of the battery employing them, depend significantly on their preparation methods, analytical methods for elucidating the complex relationship between the composite structure and battery performance were also developed[7, 8, 10]. Especially, gaining insight into the reaction distribution in the composite is key to understanding its structure and electrochemical properties. While studies attempting to gain such insights using lithium-ion charge carrier batteries have been reported, the reaction distributions were widely analyzed indirectly based on the oxidation state changes of the active materials[11, 12], mainly due to the lack of suitable analytical techniques for this purpose. The available techniques for analyzing the light element lithium are mostly limited to scanning transmission electron microscopy combined with electron energy loss spectroscopy[13, 14]. However, these techniques are not suitable for analyzing the composite electrodes with micrometer sized particles of active material and solid electrolyte.

To analyze the lithium distribution in micrometer- or larger-scale areas that are typical of practical batteries, we envisaged the use of micro-ion beam analysis. Particle-induced X-ray emission (PIXE) and particle-induced gamma-ray emission (PIGE) techniques allow high-resolution quantitative determination of the concentration distribution of lithium and other elements in a sample by scanning with an ion beam[15-17]. We reported

the first demonstration of the PIXE and PIGE analysis approaches for determination of lithium concentration distribution in sulfide-based all-solid-state battery in its prepared state[17]. Using this approach, the difference in lithium concentration among the different layers was confirmed, and the interface between the composite electrode and the solid electrolyte separator layer was identified by lithium concentration. On the other hand, the changes in lithium concentration in the composite electrode due to the electrochemical charge/discharge reaction has not been reported previously. In this paper, we report the use of a preliminary *ex-situ* PIXE/PIGE analysis of the composite electrode prior to the *in-situ* analysis, for gaining improved insights into the composite toward facilitating its better design. All-solid-state lithium batteries were prepared using $Li_{10}GeP_2S_{12}$ solid electrolytes, and the change in lithium concentration in the composite electrode after the charging process was investigated.

2. Experimental

Sample preparation processes are summarized in Figure 1. The pellet-shaped all-solid-state batteries with diameters of 10.2 mm were fabricated by uniaxial pressing at room temperature [3, 6]. The assembling process was completely conducted in an argon-filled glove box to prevent side reactions of the sulfide materials due to exposure to the ambient atmosphere. The materials used for the preparation of pellet cells, along with their weights and weight ratios are summarized in Table 1. The cathode/anode composite electrode consists of active material, solid electrolyte, and conductive carbon. $LiNbO_3$-coated (10-nm-thick) $LiCoO_2$ was used as the active cathode material, while $Li_4Ti_5O_{12}$ was used as the anode counterpart.

A pressure of 533 MPa was used to press the material to prepare the cells, and the thickness of the resulting pellets was ~910 μm. Two types of circular pellet cells were prepared in this study : an as-prepared cell (state of charge 0%, designated SOC-0) and a charged cell (state of charge 100%, designated SOC-100). The SOC-0 was divided into two semilunar SOC-0 pellets, which were then installed in gas-tight cells comprising a beam extraction window (7.5-μm-thick Kapton film)[17]. The SOC-100 was prepared by subjecting a pellet-type cell with the same configuration to a galvanostatic charging process using TOSCAT-3100 (Toyo system). A constant current of 42.7 μA (0.05C) was applied to the battery for charging the pellet to 2.6 V (*vs.* anode composite), followed by which, the battery potential was maintained at 2.6 V in a constant-voltage mode until the current decayed to less than 4.27 μA. The SOC-100 was divided and installed employing

the same process used for SOC-0 to demonstrate elemental analysis. The difference in lithium distribution between these cells was analyzed using the PIXE/PIGE technique.

Elemental distribution analysis was carried out using a 3.0-MeV proton ion beam generated from a 3-MV single-ended electrostatic accelerator at Takasaki Advanced Radiation Research Institute (TARRI) of National Institutes for Quantum and Radiological Science and Technology (QST). The diameter and current of the proton microbeam were typically 1.5 μm and 300 pA, respectively. The distance from the extraction window to the positive electrode sample was ~3 mm. The size of the obtained proton microbeam on the sample surface under these experimental conditions (*e.g.*, beam size, Kapton film thickness, distance in the air) was estimated to be ~39.2 μm by SRIM-2013 simulation[17]. While a Si(Li) detector was employed to count the characteristic X-ray emissions from germanium, cobalt, and titanium, a high-purity germanium (HPGe) detector was used to count the 478-keV gamma rays from the ^{7}Li(p, p'γ) inelastic scattering. Additional details of the condition and setting used for the measurements are described elsewhere[16, 17]. Elemental distribution data were simultaneously acquired using the PIXE and PIGE techniques by irradiating the microbeam for 30 min on a 100 μm × 100 μm square area around the interface between each electrode composite and separator layer.

3. Result and discussion

Figure 2 shows the elemental distribution mapping at the cathode/anode and separator interfaces of the SOC-0 sample. Since cobalt and titanium are not incorporated in the separator layer, the X-ray emissions from these elements are identification signals for the cathode and anode composite layers, respectively. The contrast observed in the acquired X-ray emission intensities between the cathode/anode composite and separator indicated the formation of a well-defined interface in the prepared pellet cells. Therefore, these samples could provide a suitable observation field for assessing the variations in the lithium distribution during the charging process.

The charging curve of the prepared pellet cell (Figure 3) indicates that the gravimetric charge capacity of the battery was 88.6 mAh g^{-1} based on the quantity of $LiCoO_2$ in the cathode composite. The lithium extraction amount (x in $Li_{1-x}CoO_2$) was determined to be 0.325; thus, a composition of $Li_{0.675}CoO_2$ was incorporated for the cathode composite in SOC-100. Simultaneously, the composition of anode-active material ($Li_4Ti_5O_{12}$) was varied to $Li_{5.79}Ti_5O_{12}$. Using these compositions and a lithium concentration (c_{Li}) calculated from the theoretical density, the lithium quantity, which could contribute to the

gamma-ray emission, is estimated in Table 2. The stopping range of the proton microbeam (d) is defined as the distance where the energy of irradiated proton beam decreases from 3 MeV to 1 MeV. The d value in each part of the pellet cell is calculated by SRIM-2013 using chemical composition and density values. At a depth less than the d value from the sample surface, the irradiated proton microbeam can react with lithium. The number of lithium ions (n) that react with the irradiated proton microbeam in a 1-cm^2 area at a depth d was also estimated. PIGE analysis is reportedly suitable for obtaining the difference in n values (Δn) that are larger than 0.25×10^{-4} mol[17]. However, the Δn value of anode composite between SOC-0 and SOC-100 is probably too small (~0.1×10^{-4} mol) to be detected by PIGE. Since a larger Δn value of ~0.36×10^{-4} mol was confirmed in the cathode composite, the elemental distribution at the interface between the cathode and separator was suitably analyzed.

The elemental distribution mappings at the cathode composite/separator interface of SOC-0 and SOC-100 with color visualization are shown in Figure 4 (a-d). The layout of the observed pellet cell is the same as that depicted in Figure 1. The cathode composite exists on the right side in the mapping, and the distributions in the lithium mapping detected by gamma-ray emission indicate that the cathode composites have slightly lower lithium concentration than that of the separator layer. Such a distribution is reasonable based on the number of lithium ions in each layer, indicating that the separator layer has higher lithium concentration. However, a comparison of the cathode composite between the SOC-0 and SOC-100 indicated no clear change in the lithium distribution due to the lithium extraction from the cathode composite during the charging process, which could be due to the inherent limitation of the *ex-situ* measurement. Since a comparison of the absolute value of gamma-ray intensity from lithium is difficult due to the use of different samples for the observation, the gamma-ray intensity of the lithium was normalized by the X-ray emission intensity of cobalt, because the amount of cobalt in the cathode composite is constant during the charging process. The normalized lithium distribution mappings are shown in Figure. 3 (e, f). The normalization processing reduced the lithium/cobalt intensity at the region where cobalt exists. An enhanced reduction was observed for the SOC-100 sample, corresponding to lithium extraction from $LiCoO_2$ during the charging process, which is described by the following equation: $LiCoO_2 \rightarrow Li_{1-x}CoO_2 + xLi^+ + xe^-$.

Furthermore, to consider the gradation of lithium at the interface, a line profile from the color-visualized mapping is illustrated in Figure 5. The normalized intensity overlapped for both samples from 0 to 60 pixels. The interfacial lithium/cobalt ratio between the separator and cathode composite seems comparable for the prepared samples.

Additionally, in the larger-pixel region where the cathode composite exists, the normalized intensity appears to deviate from each other due to the extraction of lithium from $LiCoO_2$. The distribution mappings for the SOC-100 sample exhibited a sharp decline in lithium distribution at the interface.

However, because the separator layer does not contain cobalt, the lithium/cobalt profile could not reflect the exact lithium concentration in this area. To evaluate the lithium concentration from the different normalization, lithium/germanium line profile is shown illustrated in Fig. 5(b). Regardless of the state of charge, the concentration in the separator region (<60 pixel) converged to a substantially constant value and overlapped in these profiles. Considering this result, the presence of the lithium/cobalt profile gradient at separator was likely to be the noise due to the slight leakage of the cobalt signal from the cathode side to the separator side. This could be due to the influence of detection spatial resolution obtained from the wide diameter of the ion beam. The normalized intensities of lithium/germanium over 60-pixel showed the same trend as those of lithium/cobalt. Therefore, the decrease in lithium concentration at the cathode layer by charging was confirmed by two different normalization approaches.

The observed gentle slope in those profiles around the interface could be due to the roughness at the observed cross-section of the samples, which may decrease the spatial resolution of the measurements. Although we have confirmed that the merged data of three times 10 minutes results are comparable to 30 minutes continuous recording data in case of the measurement for the same sample with the fixed position, it is still difficult to discuss the accuracy of the concentration gradient near the interface. There are still problems regarding the analysis of lithium distribution and quantitative discussion combining with the charge-discharge results, and it is necessary to optimize the sample preparation methods and arrangement of ion beam measurements for the interfacial structure analysis of lithium distribution. In order to obtain more accurate quantitative-ness with this method, in addition to improving the smoothness of the sample observation surface, it is considered effective to measure a known concentration standard sample with equivalent form. The reproducibility and quantitativity of the ion beam experiments for the all-solid-state battery will be demonstrated in the near future.

Overall, we reported herein, the first observation of lithium distribution and its variation in the sulfide-based all-solid-state battery using the composite electrode by the PIXE and PIGE techniques. Detailed analysis of the slope of concentration gradient depending on the composite structure and charging rate could provide the reaction distribution in the cathode composite. However, these observed structures reflect the thermodynamic equilibrium state because the samples were prepared by an *ex-situ* technique, and the

measurements were acquired after a long rest period. While these studies afford meaningful insights into the lithium-ion distribution in the composite, a study of the dynamic behavior kinetics by direct observation using *in-situ* techniques is required for better understanding of the underlying reaction mechanism of the all-solid-state lithium battery.

4. Conclusion

Microbeam PIXE and PIGE analyses of an all-solid-state lithium battery before and after charging were demonstrated herein. Lithium distribution at the cross-section of the pellet type battery was detected by microbeam PIGE. Normalized intensity mapping of lithium/cobalt revealed the change in lithium distribution near the cathode composite/separator interface. We expect that the microbeam PIXE and PIGE techniques would be powerful tools for observing the lithium distribution with micrometer-scale spatial resolution in all-solid-state lithium batteries using composite electrodes. The experimentally visualized lithium distribution in the composite cathodes can be an important design guide and a powerful diagnostic tool for next-generation batteries. Further analysis of the *in-situ* conditions to understand the dynamic behavior of lithium distribution in solid-state batteries will be reported in the near future.

References

1. Z. Gao, H. Sun, L. Fu, F. Ye, Y. Zhang, W. Luo, and Y. Huang, *Adv. Mater.* **30**, 1705702 (2018).
2. N. Kamaya, K. Homma, Y. Yamakawa, M. Hirayama, R. Kanno, M. Yonemura, T. Kamiyama, Y. Kato, S. Hama, K. Kawamoto, and A. Mitsui, *Nat. Mater.* **10 (9)**, 682 (2011).
3. Y. Kato, S. Hori, T. Saito, K. Suzuki, M. Hirayama, A. Mitsui, M. Yonemura, H. Iba, and R. Kanno, *Nat. Energy* **1**, 16030 (2016).
4. Y. Seino, T. Ota, K. Takada, A. Hayashi, and M. Tatsumisago, *Energy Environ. Sci.* **7**, 627 (2014).
5. A. Sakuda, A. Hayashi, and M. Tatsumisago, *Sci. Reports* **3**, 2261 (2013).
6. W. J. Li, M. Hirayama, K. Suzuki, and R. Kanno, *Solid State Ionics* **285**, 136 (2016).
7. Y. Kato, S. Shiotani, K. Morita, K. Suzuki, M. Hirayama, and R. Kanno, *J. Phys. Chem. Lett.* **9**, 607 (2018).
8. Y. Ito, S. Yamakawa, A. Hayashi, and M. Tatsumisago, *J. Mater. Chem. A* **5 (21)**, 10658 (2017).
9. S. Teragawa, K. Aso, K. Tadanaga, A. Hayashi, and M. Tatsumisago, *J. Power Sources* **248 (0)**, 939 (2014).
10. P. Braun, C. Uhlmann, M. Weiss, A. Weber, and E. Ivers-Tiffée, *J. Power Sources* **393**, 119 (2018).
11. M. Otoyama, Y. Ito, A. Hayashi, and M. Tatsumisago, *Chem. Lett.* **45 (7)**, 810 (2016).
12. K. Chen, S. Shinjo, A. Sakuda, K. Yamamoto, T. Uchiyama, K. Kuratani, T. Takeuchi, Y. Orikasa, A. Hayashi, M. Tatsumisago, Y. Kimura, T. Nakamura, K. Amezawa, and Y. Uchimoto, *J. Phys. Chem. C* **123 (6)**, 3292 (2019).
13. Y. Nomura, K. Yamamoto, T. Hirayama, M. Ohkawa, E. Igaki, N. Hojo, and K. Saitoh, *Nano Lett.* **18 (9)**, 5892 (2018).
14. Y. Nomura, K. Yamamoto, T. Hirayama, S. Ouchi, E. Igaki, and K. Saitoh, *Angew. Chem. Int. Ed.* **58 (16)**, 5292 (2019).
15. K. Mima, R. Gonzalez-Arrabal, H. Azuma, A. Yamazaki, C. Okuda, Y. Ukyo, H. Sawada, K. Fujita, Y. Kato, J. M. Perlado, and S. Nakai, *Nucl. Instrum. Methods Phys. Res., Sect. B.* **290**, 79 (2012).
16. A. Yamazaki, Y. Orikasa, K. Chen, Y. Uchimoto, T. Kamiya, M. Koka, T. Satoh, K. Mima, Y. Kato, and K. Fujita, *Nucl. Instrum. Methods Phys. Res., Sect. B.* **371**, 298 (2016).

17. K. Yoshino, K. Suzuki, Y. Yamada, T. Satoh, M. Finsterbusch, K. Fujita, T. Kamiya, A. Yamazaki, K. Mima, M. Hirayama, and R. Kanno, *Int. J. PIXE* 1850002 (2018).

Table 1 Configuration of the pellet cells prepared in this study.

	Material	Weight ratio (%)	Quantity (mg)
Cathode composite	$LiNbO_3/LiCoO_2$	60	10.4
	$Li_{10}GeP_2S_{12}$	34	
	Acetylene black	6	
Separator	$Li_{10}GeP_2S_{12}$	100	80.1
Anode composite	$Li_4Ti_5O_{12}$	30	34.8
	$Li_{10}GeP_2S_{12}$	60	
	Acetylene black	10	

sss

Table 2 Relative density, lithium concentration, stopping range, and number of lithium ions in each region of the all-solid-state battery prepared in this study.

Component	Sample state	Density ρ (g cm^{-3})	Lithium concentration c_{Li} (mol cm^{-3})	Stopping range d (μm)	Number of lithium ions n (mol)
Cathode composite	SOC-0	1.91	0.0227	95.69	2.17×10^{-4}
	SOC-100		0.0189		1.81×10^{-4}
Separator	SOC-0/SOC-100	2.05	0.0279	87.76	2.45×10^{-4}
Anode composite	SOC-0	1.29	0.0165	136.4	2.25×10^{-4}
	SOC-100		0.0172		2.35×10^{-4}

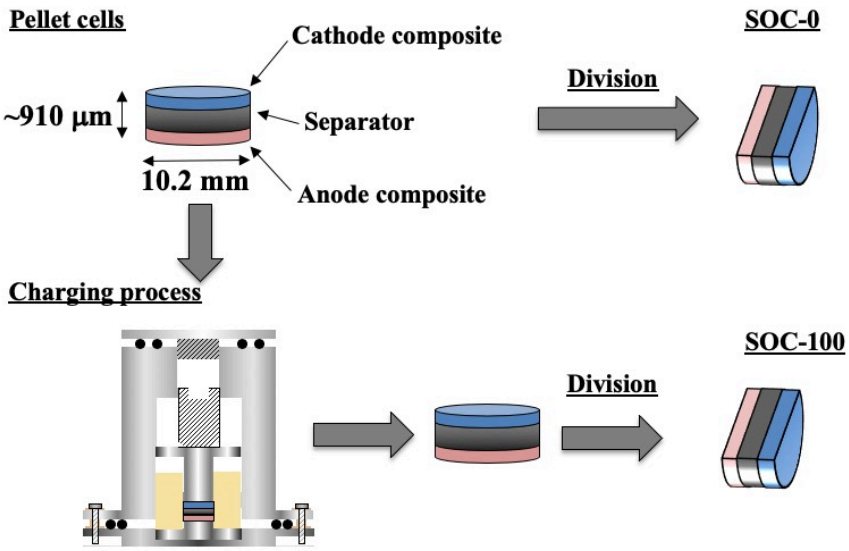

Figure 1 Sample preparation of the pellet cells for SOC-0 and SOC-100.

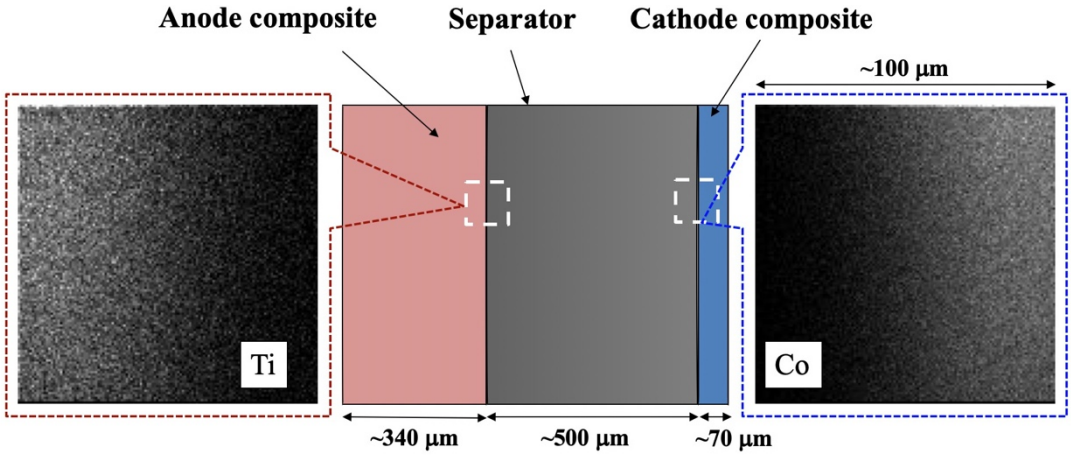

Figure 2. Schematic of the analyzed pellet cell sample and the cross-section PIXE analysis results of titanium and cobalt, respectively, for anode and cathode composites of the SOC-0 sample. The elemental mapping area equals to 100 µm × 100 µm.

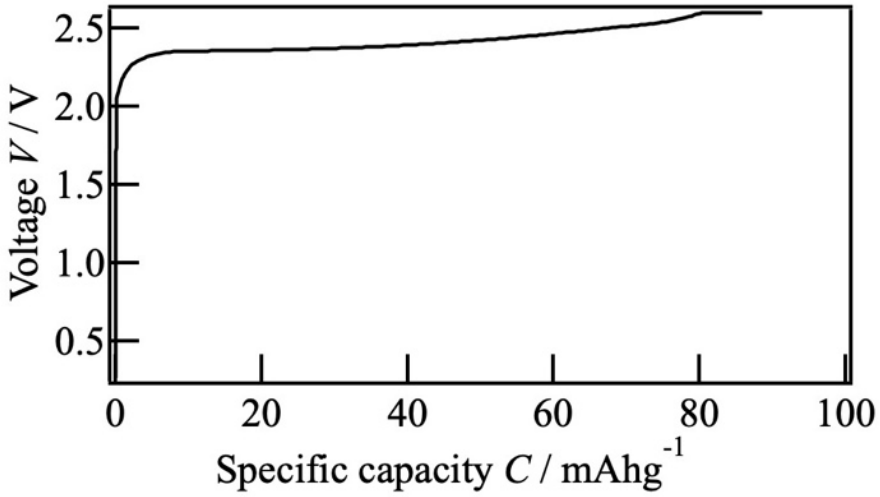

Figure 3 Initial charging curve of the all-solid-state lithium battery prepared in the present study. The specific capacity was calculated based on the weight of $LiCoO_2$ in the composite cathode.

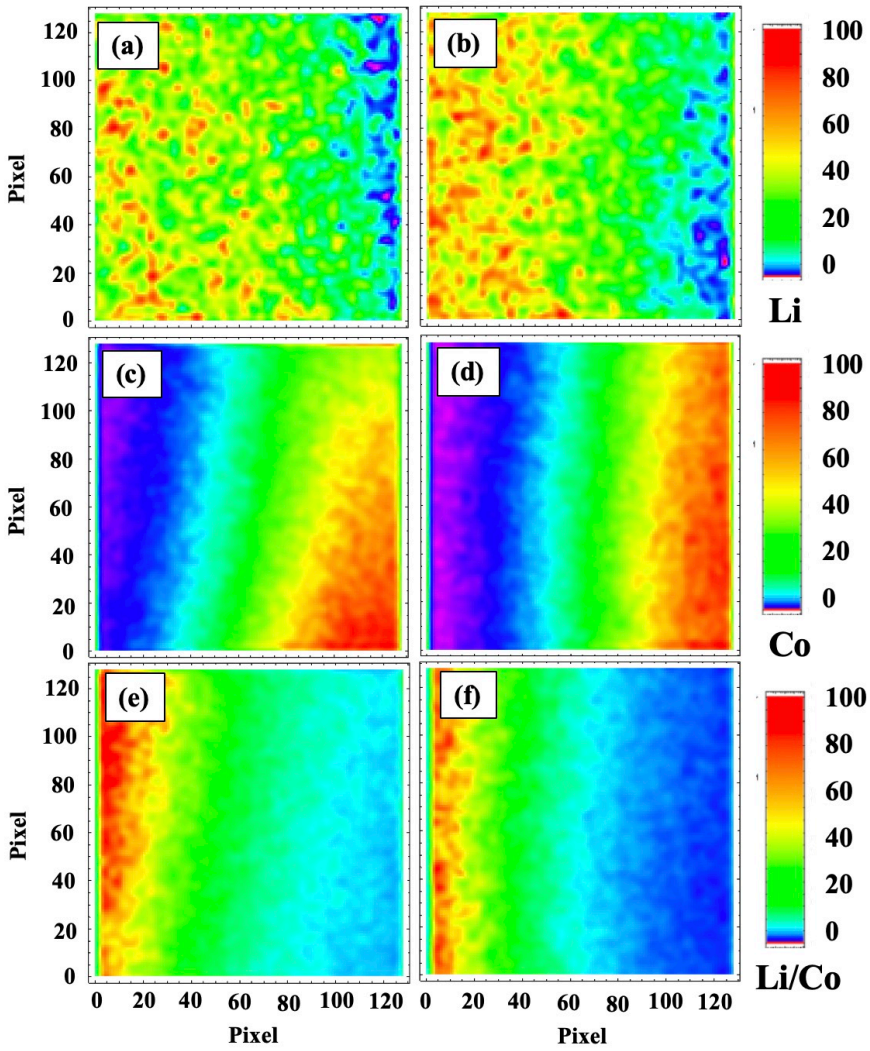

Figure 4. Color-visualized elemental distribution mappings of lithium (a, b), cobalt (c, d), and normalized lithium/cobalt (e, f). Left panels and right panels indicate SOC-0 and SOC-100, respectively. The elemental mapping area equals 100 × 100 μm^2.

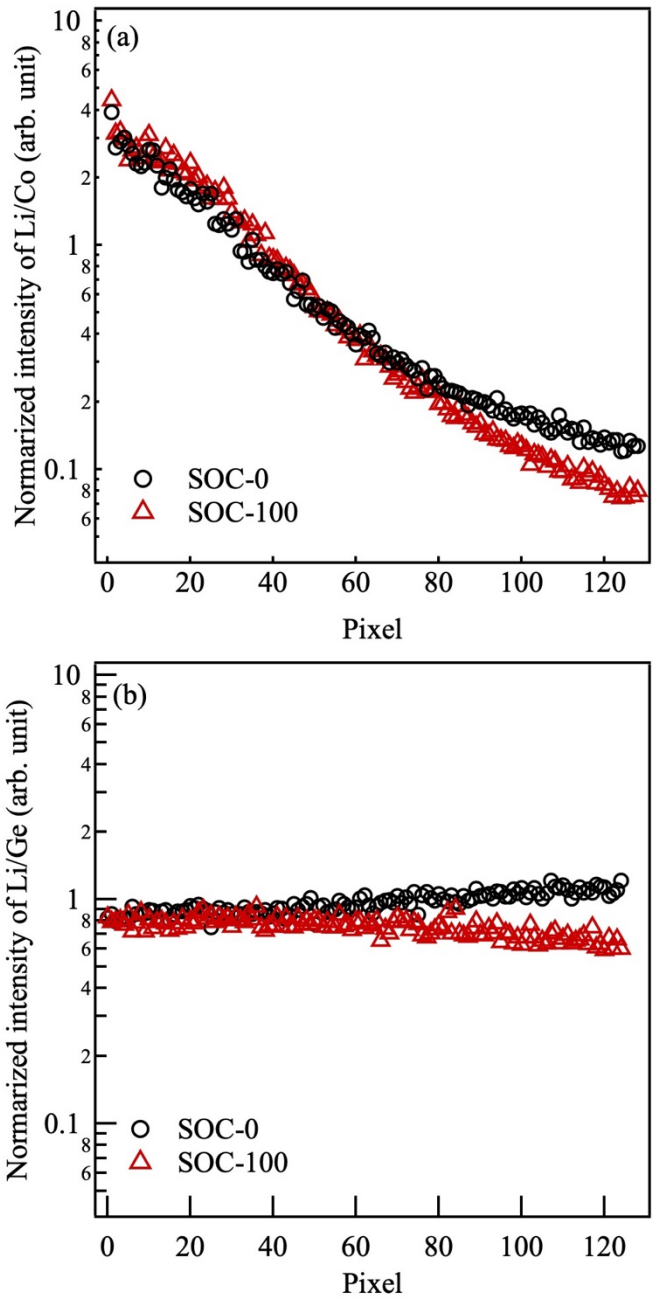

Figure 5. Line profiles of the lithium/cobalt (a) and lithium/germanium (b) mapping. 128 pixels in the x-axis correspond to 100 μm in the cross-sectional image.